Nanoparticle-based 3D membrane for impedimetric biosensor applications

Lu Cao, Janice Kiely, Martina Piano and Richard Luxton*

Institute of Bio-Sensing Technology, University of the West of England, Frenchay Campus, Bristol, BS16 1QY

E-mail: Lu2.Cao@live.uwe.ac.uk (Lu Cao)

Abstract:

This paper reports on a comparison between nano-ZnO/CuO and nano-ZnO nitrocellulose membrane biosensors, both of which were fabricated using a simple and inexpensive sonication technique. To produce the nano-ZnO/CuO membranes, the technique involved sonication of 1% (w/v) ZnO and 1% (w/v) CuO nano-crystal colloidal suspensions, with a volume ratio of 1:2. The membranes were analysed by scanning electron microscopy and energy-dispersive spectroscopy, which showed the gradated distribution of nanoparticles in the membrane. Impedance spectroscopy demonstrated that the sonication resulted in a greater than two-fold enhancement of the output signal. Changes in impedance phase values, at a frequency of 100 Hz, were used to establish dose dependent responses for C-reactive protein (CRP). Limits of detection of 27 pg/mL for the 1% (w/v) nano-ZnO and 16 pg/mL for the 1% (w/v) nano-ZnO/CuO nitrocellulose membrane biosensors were demonstrated.

Keywords

ZnO/CuO nitrocellulose membrane; impedance spectroscopy; phase change; CRP detection

1. Introduction

The drive to develop technology that can be used to diagnose and monitor disease in the community has seen the application of biosensing technology to measure a wide range of biomarkers. Biosensor technology enables the rapid measurement of biomarkers at the point of test, thereby allowing a medical decision on the management and/or treatment of a patient to be made immediately. Antibody-based biosensors are well suited these applications, due to their ability to deliver high specificity and sensitivity, as well as being adaptable for detection of a wide range of analytes. For example, antibody-based biosensors have been developed for detection of the following: cardiac troponin-T (cTnT) [1], epidermal growth factor receptor (EGFR) [2], cortisol [3], brain natriuretic peptide (BNP) [4], Aflatoxin B1 (AFB1) [5] and insulin [6] (supporting information **Table S1**). A number of antibody-based biosensors have also been developed for measurement of C-reactive protein (CRP) [7–9]. CRP is a biomarker that, when elevated from a concentration of 1 mg/L to a level of, or above, 3 mg/L, indicates an infection or other active inflammatory process. CRP is synthesised in the liver and released in response to inflammatory changes. It is regulated by interleukin-6, interleukin-1β and tumour necrosis factor-α [10] and is thought to be a key biomarker of systemic inflammation [11].

Numerous biosensor fabrication processes are described in the literature, but in recent years, there has been much focus on the application of nano-materials, including the use of metal oxide nano-crystals, such as zinc oxide (ZnO). ZnO is a functional n-type semiconductor, with a wide band gap of 3.37 eV at room temperature [12]. Distinctive features of ZnO include good electrical transport, good biocompatibility, cost effectiveness, chemical stability and a high isoelectric point, allowing better absorption of biomolecules by electrostatic interactions [13,14]. In addition, the benefits of utilising nanostructures to form a biosensor surface include the high surface area, the effect of nano-confinement to enhance biosensor sensitivity and the ability to tailor the particles/surface in a controlled manner to adapt nanostructure biosensors for detection of a range of analytes [1,13,15]. Shen et al. developed a series of thin film transistor (TFT) biosensors for detecting biomarkers of tumours [2]. They applied anti-EGFR antibodies to a ZnO nano-surface to detect

EGFR [2]. The electrical charge on the sensing pad was modified by proteins, inducing corresponding charges in the TFT forming a conducting channel and increasing the current output with changes in the concentration of EGFR [2]. This study showed that, compared with the TFT biosensor without ZnO nanorods, a device with nanorods had a 4.7 times enhanced output because the ZnO nanorods helped to attract proteins due to the possession of more static charges and a larger surface-to-volume ratio [2]. Copper Oxide (CuO) is a p-type semiconductor with a narrow band gap of 1 eV to 1.57 eV [16]. The improvement in sensing performance of ZnO/CuO composites has been attributed to many factors, including increased interfacial potential barrier energy associated with the formation of p-n junctions resulting in a higher resistance and an enhanced surface area to support greater antibody loading [17].

Various methods for fabricating ZnO and CuO nanostructures, with and without substrates, have been reported. A relatively simple and inexpensive way is to fabricate ZnO and ZnO/CuO films involves sonication. Choosing suitable solvent media and dispersing agents during sonication helps interrupt the binding forces between individual particles by combining both chemical and physical approaches [18]. The sonication power results in improved dispersal of the colloidal suspension. Zhang et al. described a method for preparing titanium dioxide (TiO_2)-modified carbon paste electrodes [19]. Firstly, the titanium dioxide hollow microsphere colloid powder was added to Britton–Robinson buffer solution and sonicated to produce a well-dispersed colloid solution. Then the well-dispersed solution was dropped on to a surface and dried in air. Lastly, the electrodes were washed with ultrapure water [19]. Al-Hinai et al. demonstrated that ZnO nanoparticles in deionized water could be dispersed by probe sonication, followed by magnetic stirring for 24 h, and then mixing with Polyethersulfone (PES) dissolved in 1-Methyl-2-pyrrolidone (NMP) and stirring for a further 24 h [20]. The nanoparticles were then cast on a flat glass plate in a water bath overnight to hydrothermally produce ZnO nanorods [20]. Lee et al. fabricated a platform for biocompatible antibacterial applications using ultrasound-assisted sonochemistry to fabricate a flexible ZnO nanopillar array film within 5 min [21]. The method utilised extremely high temperature (>5000 K), pressure (>200 MPa), and cooling rate ($>10^7$ K^{-1}) in a liquid medium under sonication [21].

A number of researchers have recognised the benefits of ZnO/CuO composites in biosensor fabrication. Widiarti et al. found that the addition of CuO decreased the band gap energy of the composite and observed that this enhanced the antibacterial activity [22]. They speculated that this was due to electrons being easily excited from the valence band to the conduction band, causing the formation of reactive oxygen species and superoxides [22]. In addition, it was suggested that CuO-ZnO composites demonstrated enhanced antibacterial activity due to the presence of Zn^{2+} ions and the generation of reactive oxygen species causing bacterial membrane lipid peroxidation. [22,23]. Reported advantages of biosensors fabricated using ZnO/CuO composites compared with ZnO nanostructures include improved linear range, lower limits of detection, shorter response times and greater sensitivities [24,25]. Sonication has also been shown to have benefit in relation to fabrication of ZnO/CuO biosensors. Our research group has investigated the fabrication of biosensors formed from ZnO/CuO nano-crystals coated on polyethylene terephthalate (PET) substrates [26,27]. In this work, we achieved improved reproducibility in fabricating ZnO/CuO nano-surfaces by sonicating 1% (w/v) ZnO and 1% (w/v) CuO nano-crystal suspensions [26,27]. Optimum signal output was achieved with mixed suspensions in volume ratios 1:2 (ZnO:CuO) [26].

Three-dimensional membranes are widely used in biosensing. Recently their utilisation alongside ZnO nanoparticles has been reported. For example, Al-Hinai et al. grew ZnO nanorods on the top surface of a PES membrane on a flat glass plate to form a biosensor [20]. Munje et al. developed a flexible biosensor, including a ZnO thin film active region by deposition of nanoparticles on to a nanoporous polyamide membrane. This methodology enhanced the diffusion time associated with the mass transport within the nanopores and provided a high surface to volume ratio to enhance the detection capability [28]. Munje et al. utilised a nano-porous ZnO thin film as an active sensor substrate, noting that the electrical double layer formed at the liquid-semiconductor interface was amplified in the presence of the nano-porous substrate with an associated enhancement in charge accumulation [3]. However, there have been no previous reports of impregnating a porous membrane with ZnO (or CuO) to form the active layer of a biosensor, as described in this paper.

Here we report on the fabrication and evaluation of nano-ZnO and nano-ZnO/CuO nitrocellulose membrane biosensors, formed using a colloidal sonication technique. The biosensors are label-free and non-faradaic, i.e. there is no charge transfer between the biomolecule complex and the sensor electrodes [4]. In this study, we analysed the membranes using scanning electron microscopy (SEM) and energy-dispersive spectroscopy (EDS) analysis and we characterised performance of the biosensors by the measurement of CRP using impedance spectroscopy. For non-faradaic impedimetric biosensors, at the liquid-semiconductor interfaces, the electrical double layer forms a large interfacial capacitance with high density of charge accumulation [3]. This capacitance changes actively with the concentration of biomolecular binding [3] and in this work, excellent limits of detection for the biosensor are demonstrated.

2. Materials and Methods

2.1 Membrane Preparation

Fabrication process for the 1% nano-ZnO nitrocellulose membranes: - In our work, 0.6 g ZnO nanoparticles (ZnO, 99.9+%, 80 - 200 nm from US Research Nanomaterials Inc.) were added to 60 mL double-distilled water. 1% ZnO suspension was stirred for one hour at room temperature. A 1% (w/v) ZnO suspension was stirred for 1 h at room temperature. Nitrocellulose blotting membranes (Sartorius) with 0.45 μm pore size were cut using a Biodot guillotine to form a 15 mm × 15 mm square. A number of the membranes were immersed in the ZnO colloidal suspension and sonicated for 15 min in a sonication bath (Langford Ultrasonics) with a power of 300W at 40 Hz. Other membranes were immersed for 15 min without sonication for comparison. Finally, all the membranes were rinsed in deionised water 3 times and dried in sealed box with silica gel before being used for the immobilisation of antibody.

Fabrication process for the 1% nano-ZnO/CuO nitrocellulose membranes: - In the process 0.2 g ZnO nanoparticles and 0.4 g CuO nanoparticles (CuO, 99.5+%, width 10 - 30 nm, Length: 200 – 800 nm from US Research Nanomaterials Inc.) were added to 60 ml double deionized water. 1% ZnO (w/v) was mixed with 1% CuO (w/v) nanopowders in water for 1 h to give 1:2 (v/v)/(wt%:wt%) ZnO/CuO colloidal suspension. Nitrocellulose membranes were then soaked in the ZnO/CuO suspension and subjected to sonication for 15 min as described above; other membranes immersed for 15 min were without sonication for comparison. Finally, the membranes were rinsed using deionised water 3 times and dried in atmosphere with silica gel before being coated with antibody.

2.2 Characterization of Membranes

The cross section of a nanoparticle nitrocellulose membrane was prepared using a double edge razor blade and examined using a FEI Quanta 650 field emission scanning electron microscope (ESEM) with Everhart-Thornley Detector (ETD). The morphology of cross sections of untreated nitrocellulose membranes, a nano-ZnO

nitrocellulose membrane and a nano-ZnO/CuO nitrocellulose membrane, were analysed. To perform the SEM analysis, samples were mounted on an aluminium stud and coated with a thin layer of Au using an Emscope SC500 Gold sputter coating unit prior to analysis. For the ZnO/CuO nitrocellulose membrane, a Gaseous Secondary Electron Detector (GSED), with a high pressure at 3 Torr, was also used in the SEM.

EDS (Oxford Instruments AZtec EDS) was used to analyse the chemical compositions of the sonicated nano-ZnO and nano-ZnO/CuO nitrocellulose membranes.

2.3 CRP Sensor Fabrication and CRP Assay

To prepare the membranes for the assays, 40 µl (200 ng) of monoclonal mouse anti-human C-reactive protein (4C28, from HyTest Ltd, Turku, Finland) was diluted in 5 mM phosphate buffered saline (PBS) at pH 7.4 (OXOID Microbiology products). The capture antibody was immobilised on to the nitrocellulose membranes (from the upper side to lower side) until it was fully wet. The anti-CRP antibody was readily immobilised in the membrane through electrostatic interaction as the ZnO nanostructures distributed within the nitrocellulose membrane were positively charge (as the pH of the buffer was 7.4 and the isoelectric point of ZnO and CuO is around 9.5 [29,30]), whereas the anti-CRP antibody used in this study is predominantly negatively charged. The membranes were then dried in a desiccator with silica gel at 4 °C overnight for 18 h. Anti-CRP antibody is immobilised on membrane not only through electrostatic interaction, but also other physical absorption processes, such as hydrophobic interactions and van der Waal's forces, forming non-covalent interactions. Wang et al. schematically presented the capacity of antibody immobilization on 3D matrix compared with a conventional 2D surface, to illustrate that it is much higher, shown in **Schematic 1** [31]. This work confirmed that the quantity of effective antibodies per unit area sharply increases from 2D to 3D immobilisation [31].

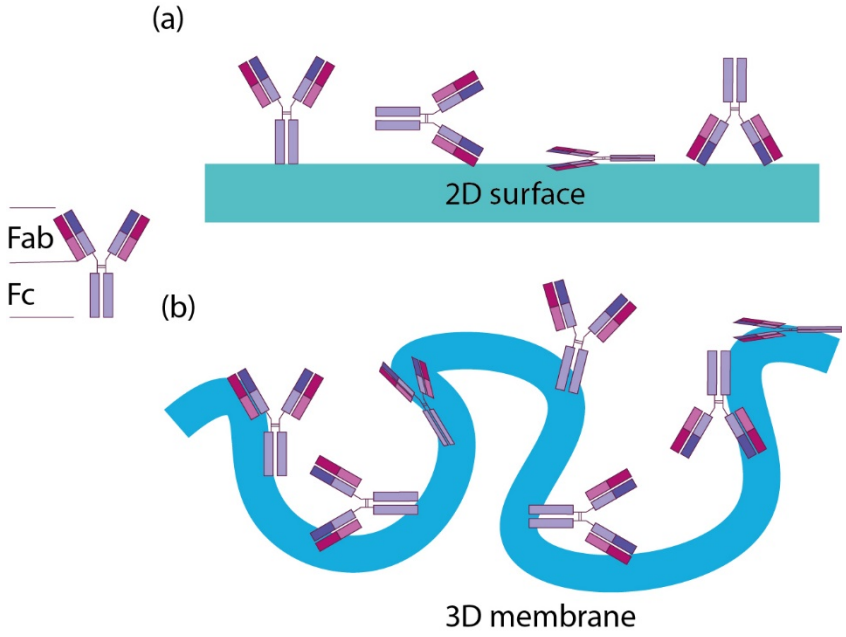

Schematic 1. Random immobilization of capture antibody (a) on a 2D surface and (b) on a 3D membrane. (Adapted from [31])

After the overnight incubation, the nano-particle nitrocellulose membranes were repeatedly (4 times) immersed in 5 mM PBS and then blocked with 1% (w/v) skimmed milk for 30 s.

Human C-reactive protein (CRP) (8C72, from HyTest Ltd, Turku, Finland) was diluted in 5 mM PBS. Then, 40 µl of CRP at different concentrations were placed on the membranes to facilitate a slow liquid absorption in to the membrane until it was fully wet. The specific concentrations of CRP were as follows: 0 (PBS only), 0.1, 0.5, 1, 5, 10, 15 ng/mL.

During the impedance testing, the membranes were laid on a glass coverslip (from Deltalab, 22 mm × 22 mm and 0.13 - 0.16 mm thick), and positioned on a 23 mm diameter D-shape electrode pair with 1 mm gap, with the lower layer and hence the highest density of nanoparticles closest to the electrode. (The gradated porosity and associated variation in nanoparticle density are described in section 3). A second coverslip was placed on top of the membrane to prevent evaporation during the measurement. The schematic diagram of the arrangement is shown in **Schematic 2**. The impedance amplitude and phase angle were measured and analysed after 10

minutes incubation time with the added CRP. The impedance values were recorded at each concentration of antigen, with 3 replicates of the nano-particles/nitrocellulose membranes, measured from 10 Hz to 4 MHz.

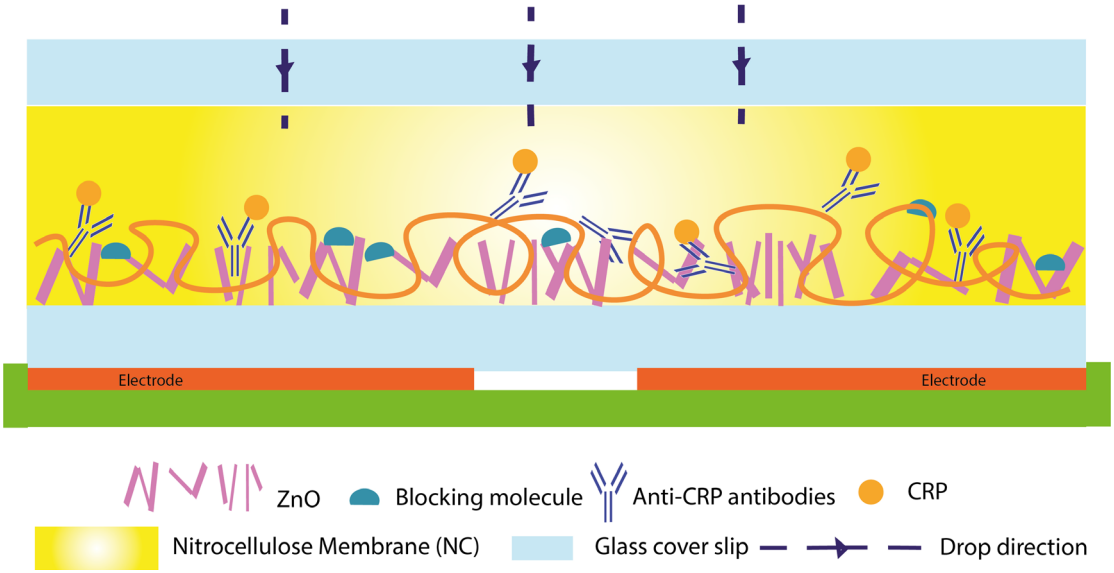

Schematic 2. Illustration of the ZnO nanoparticle nitrocellulose membrane sandwiched between two coverslips positioned above the electrodes.

A Cypher Instruments C60 Impedance-Amplitude-Phase Analyser was used to measure the impedance change of the nano-particles nitrocellulose membranes associated with antibody/antigen interactions. The frequency was scanned from 10 Hz to 4 MHz, with 300 test points, at an AC peak-to-peak voltage of 2 V with a DC offset of 0.9 mV. The impedance plots were analysed by Cypher Graph V1.21.0, Impedance Amplitude and Phase Analyser graphing application software. The change of impedance amplitude and phase angle was evaluated as function of antigen (CRP) concentration in the buffer. Rather than correlate the overall impedance to different concentrations of CRP, we determined a single frequency to give the maximum relative changes and a stable reading [4]. The sensor responses were taken at a frequency of 100 Hz. Phase changes with ZnO and ZnO/CuO (1:2) nanoparticle nitrocellulose membrane were compared with or without sonication. The phase change was defined as the difference of the impedance phase value of the biosensor

after 10-min incubation with CRP and the phase angle of the control. Results were plotted using a logarithmic scale on the x-axis.

2.4 Statistical Analysis

A 4-parameter linear-log logistic curve, with the error bars, was created using R. The estimated limit of detection (LoD) was defined as the mean of the intercept on the y axis of the calibration curve, plus 3 times the standard deviation of the intercept and calculated using R. The mean value and Standard deviation of the "intercept" at the working zero found using the 4-parameter logistic curve.

The coefficient of variation %CV = (Standard Deviation/Mean*100) was used to demonstrate reproducibility for each membrane type.

A Wilcoxon rank sum test was used to analyse the differences in phase changes between ZnO and ZnO/CuO (1:2) nano-membranes with and without sonication at each concentration, the level of significance was defined as $p<=0.05$. Analysis was performed using R.

3. Results and Discussion

3.1 Characterization of Membrane

The nitrocellulose membranes used in this study showed gradated porosity (**Figure 1**) and, as seen in the scanning electron micrograph of **Figure 1**(a), can be divided into three layers. The upper layer has the smallest pore sizes and structures shown in **Figure 1(b)**, whereas the lower layer has a loose pore structure between the white support matrix as shown in **Figure 1**(d). The horizontal lines visible in the white fillers indicate the cutting direction of the nitrocellulose membrane. The nitrocellulose membrane is manufactured by casting the nitrocellulose in solvents, which causes the significant asymmetry in the porous structures due to the evaporation of solvent [32].

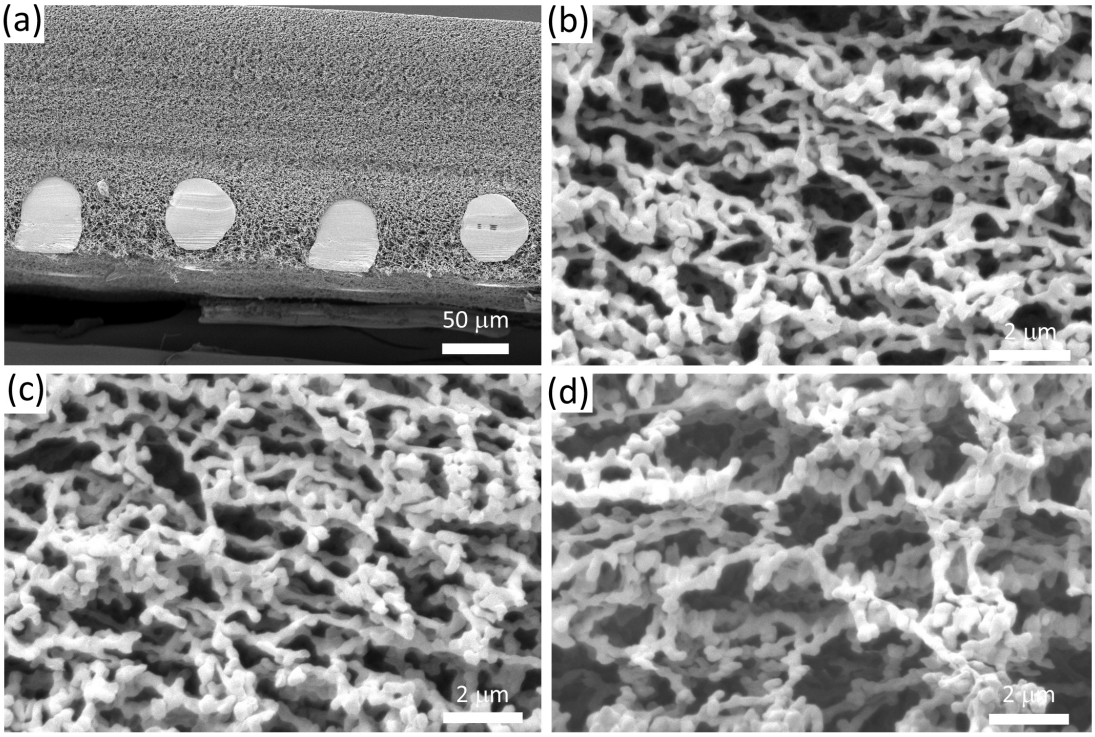

Fig. 1. Scanning electron micrographs of the nitrocellulose membrane cross-section: (a) whole cross section at 1,000× magnification; (b) upper layer of nano-ZnO/nitrocellulose membrane (with small pore structures) at 30,000× magnification; (c) middle layer of nano-ZnO/nitrocellulose membrane (with bigger and loose pore structures) at 30,000× magnification; (d) lower layer of nano-ZnO/nitrocellulose membrane (with biggest pore structures) at 30,000× magnification.

During the fabrication of the nano-particle nitrocellulose membranes, the membranes were incubated in nano-particle colloidal suspensions. **Figures 2**(a) to **2**(c) show scanning electron micrographs of the three layers of the nitrocellulose membrane. A smaller number of nanoparticles entered the upper structure due to the lower porosity, as seen in **Figure 1**(a). The nanoparticles easily entered the lower layer of the membrane as seen in **Figure 1**(c) by the force of sonication and then diffused into the middle layer, as shown in **Figure 1**(b). **Figure 2**(c) clearly shows a high number of the columnar wurtzite structures of the ZnO nanoparticles in the lower layer of the nitrocellulose membrane.

Imaging of the conductive nano-ZnO/CuO nitrocellulose membrane was performed using a Gaseous Secondary Electron Detector, as the CuO particles became charged under normal SEM conditions (seen as lighter areas at nano-crystal margins), and are shown in **Figures 2**(d) to **2**(f). As with the ZnO membranes, **Figures 2**(d) **to 2**(f) show an increasing number of ZnO and CuO nanoparticles distributed within the membrane, with the highest density of the CuO nanoparticle flakes and columnar wurtzite structure of ZnO in the lower layer of the nano-ZnO/CuO membrane. **Figure 2** also reveals that the ZnO/CuO nanostructures formed a larger number of voids compared with ZnO, which is beneficial for the antibody capture.

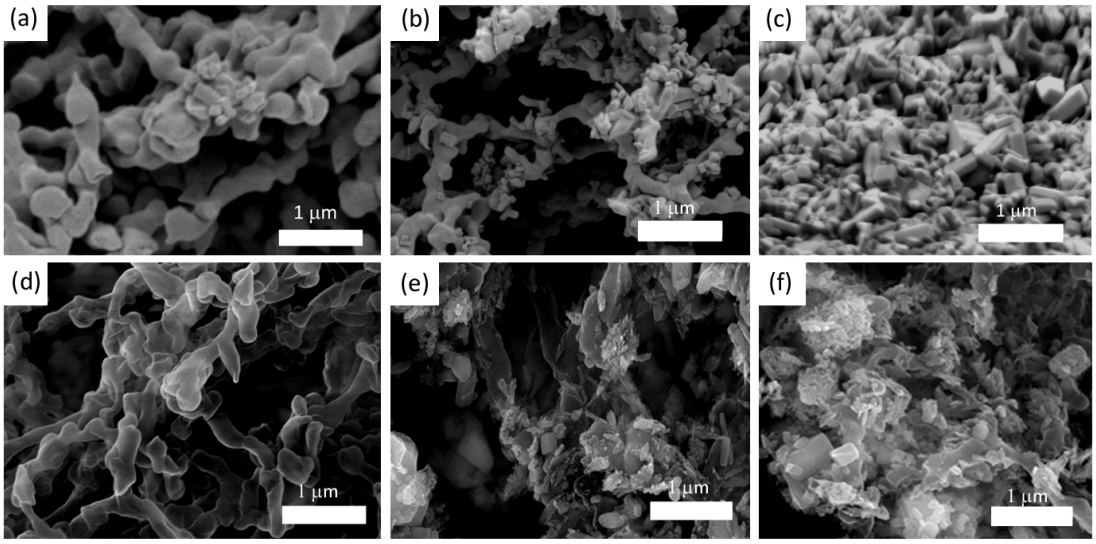

Fig. 2. Scanning electron Micrographs of nano-ZnO nitrocellulose membrane cross-section at 80,000× magnification: (a) upper layer; (b) middle layer; (c) lower layer. Scanning electron Micrographs of nano-ZnO/CuO nitrocellulose membrane cross-section at 80,000× magnification: (d) upper layer; (e) middle layer; (f) lower layer.

3.2 EDS Results

From the scanning electron micrographs, both ZnO and CuO nanoparticles were observed to be densest in the lower layer of the membrane, so the EDS analysis was performed on the lower layer. The result of atomic composition analysis by EDS on the cross-section of the nano-ZnO and nano-ZnO/CuO nitrocellulose membrane is shown in **Figure 3** and **Figure 4**. The following elements were detected: C, (Cu,) O, Zn and Au. **Figure 3** shows the results for zinc; 5(a) is the SEM image, 5(b) is the EDS spectrum and in **Figure 3**(c) the yellow areas show the regions where the Zinc is concentrated. **Figure 4** shows the results of the EDS analysis on the ZnO/CuO membrane. The distribution of the 6 elements within the lower layer of the nitrocellulose membrane is shown in **Figure 4**(b). The intensity of the coloured areas highlights the element location and loading within the matrix. The nanoparticle density was greatest between the fibres of the support matrix of the membrane, which also had the largest pore size within the layer. A small amount of Al was detected at the edge of the membrane, from the SEM stub. Referring to **Figure 4**(a), the carbon originates from the nitrocellulose and Au from the sputtered layer used in the sample preparation. The grayscale intensity of the zinc and copper in **Figure 4**(a), had a ratio of Zn to Cu 1:2.08, corresponding to 1:2 ratio of ZnO/CuO in the original nanoparticle colloid suspension. This confirmed that the fabrication methodology resulted in proportional absorption in to the membrane of the ZnO and CuO nanoparticles.

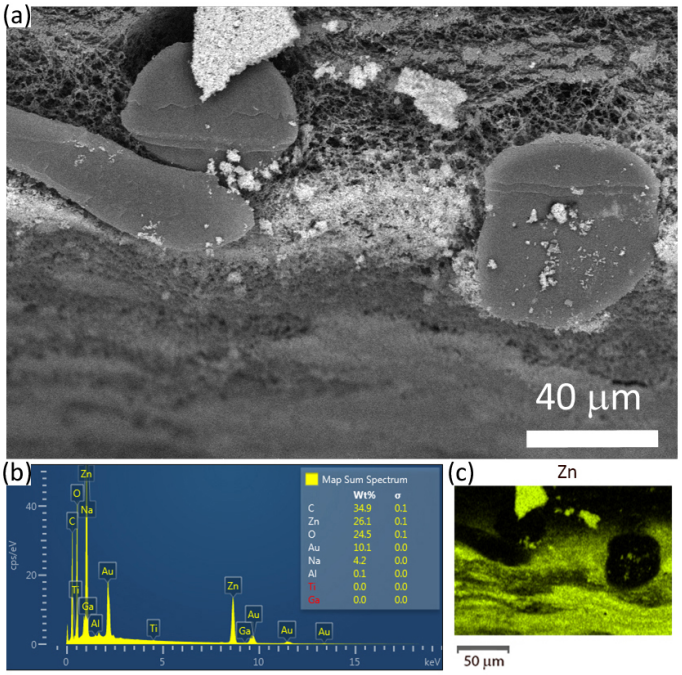

Fig. 3. SEM/EDS spectrum/mapping showing the distribution of Zn on the lower layer cross-section of the nano-ZnO membrane: (a) SEM image; (b) EDS spectrum and (c) EDS mapping of the elements of Zn.

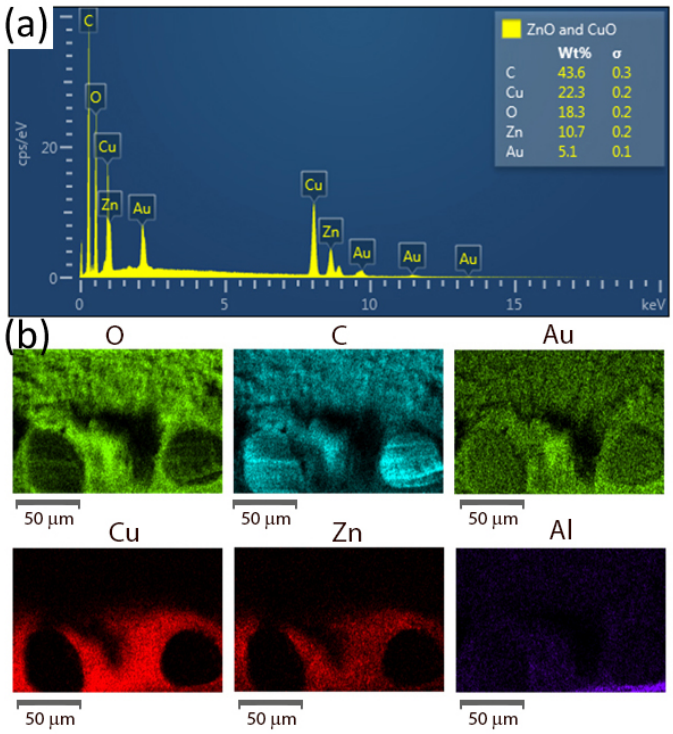

Fig. 4. EDS spectrum/mapping on the lower layer cross-section of the nano-ZnO/CuO membrane: (a) EDS spectrum and (b) EDS mapping of the elements: O, C, Au, Cu, Zn and Al.

3.3 Calibration Curves Using Different Nano-membranes with Capture Antibody

Figures 2(d) to **2**(f) and **Figure 4**(b) evidence that the ZnO/CuO nanoparticles are distributed within the porous membrane following sonication. The cross section of the biosensor developed in this study is schematically depicted in **Schematic 2**. This shows the sensing nanoparticle nitrocellulose membrane with antibody coating, which is sandwiched between two glass cover slips and positioned above two electrodes. The electrodes face the lower layer of the membrane, which was loaded with nanoparticles for capturing biological molecules. Impedance spectroscopy was used to quantify binding of CRP to the antibody on the nano-ZnO/CuO membranes, with and without sonication, and the nano-ZnO membranes, with and without sonication, for these non-faradaic biosensors.

The impedance was recorded for CRP concentrations between 0 ng/ml and 15 ng/ml, with 3 replicate nano-ZnO and ZnO/CuO membranes with or without sonication and with or without antibody immobilised, over the frequency range 10 Hz to 4 MHz (bode plots are shown in the supporting information **Figure S1-2**). In this study the most significant changes were observed below 1 kHz, around 100 Hz. This observation concurred with other published work. Selvam et al. measured the impedance of their non-faradaic biosensor over the frequency range 100 Hz to 1 MHz and found the changes to the double layer capacitance were most significant at frequencies less than 1 kHz [4]. Kinnamon et al. selected 100 Hz for their calibration dose response, as this maximised the percentage change in impedance relative to the baseline measurement, performed post-antibody functionalization [33].

Figure 5 shows the impedance amplitude and phase values measured on both the nano-ZnO membranes and the nano-ZnO/CuO membranes with different concentrations of CRP after a 10-min incubation at 100 Hz, the mean of 3 replicates. For both the nano-ZnO membranes and the nano-ZnO/CuO membranes, the

impedance decreases with CRP concentration. As both ZnO and CuO are semiconducting materials, an electrical double layer is formed when they interact with the liquid electrolytes, resulting in charge accumulation at the interface region. When binding of the CRP molecules (~116 kDa) to the antibodies occurs adjacent to this interface, the double layer capacitance is enhanced, resulting in the observed change in the impedance. Note that in **Figure 5**C, the error bars of impedance response on nano-ZnO/CuO membranes look large compared with the other plots. This is due to the fact that the range of the impedance change is small, thus the scale is magnifying the error bars. From **Figure 5**, the lines of best fit have lower residuals for the phase angle compared with the amplitude of the impedance. Consequently, subsequent calibration curves were plotted using the change in the absolute phase relative to the PBS control using a logarithmic scale on the x-axis.

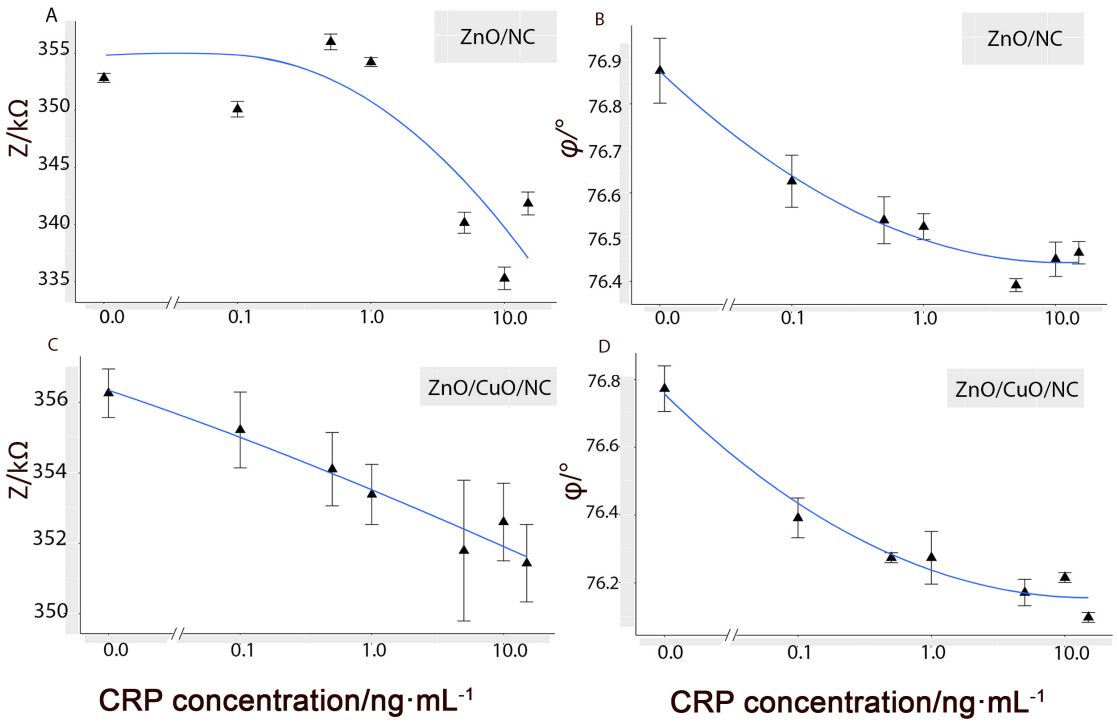

Fig. 5. Impedance amplitude/kOhms (Z/kΩ) and phase change/degree (φ/°) on nano-ZnO nitrocellulose membranes (n=3) and nano-ZnO/CuO nitrocellulose membranes (n=3) after a 10-minute incubation time with increasing concentrations of CRP, measured at a frequency of 100 Hz.

Figure 6 shows the phase change for six different nano-particle/nitrocellulose membranes at a frequency of 100 Hz. In **Figure 6**, the average phase change of samples fabricated without the sonication stage (the red bar represents nano-ZnO membrane and the light blue bar represents nano-ZnO/CuO membrane) is lower compared with the phase change for samples prepared with sonication (the green bar represents nano-ZnO membrane and the pink purple bar represents nano-ZnO/CuO membrane). The phase change for nano-ZnO/CuO membrane after sonication approximately doubles compared with no sonication, whereas for the nano-ZnO membrane there is an approximate 3-fold increase. This indicates that the sonication has a greater effect on ZnO nano-particles than on the ZnO/CuO mixture in terms of signal enhancement. These results demonstrate the importance of the sonication process in the fabrication of the biosensor. However, despite this, the ZnO/CuO membranes remain superior in terms of the amplitude of the signals relative to the control. The sonication had a highly significant effect on the signal generated from the membranes ($p<0.0005$ by Kruskal-Wallis chi-squared test).

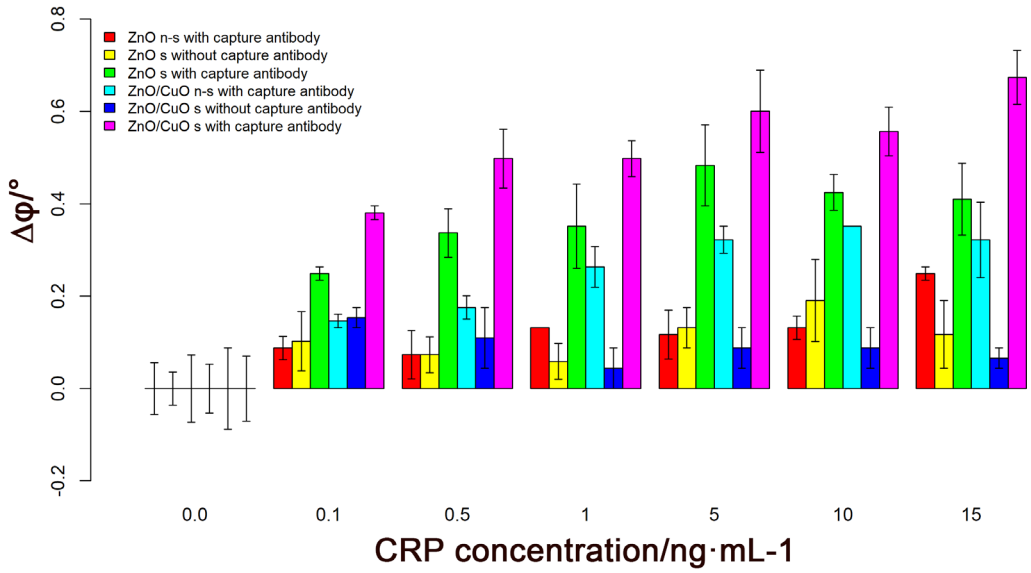

Fig. 6. Impedance phase change/degree (Δφ/°) response to seven concentrations of antigen (CRP) on the six different types of membrane. For the 3 nano-ZnO

membranes (n=3): with 200 ng capture antibody and without sonication (red), without capture antibody and with sonication (yellow) and with 200 ng capture antibody and with sonication (green). For the 3 nano-ZnO/CuO membrane (n=3): with 200 ng capture antibody and without sonication (light blue) and without capture antibody but with sonication (dark blue), with 200 ng capture antibody and with sonication (pink purple).

Table 1 shows pairwise comparisons, using a Wilcoxon rank sum test, on four types of membranes with antibody immobilised. The phase responses of the nitrocellulose membranes show a significant difference between sonicated and non-sonicated membranes for both the nano-ZnO and ZnO/CuO membranes ($p<0.05$).

Table 1. The significant differences in the membrane treatment analyzed by a Wilcoxon rank sum test among four different nano-particles/nitrocellulose membranes with antibody immobilised.

A Wilcoxon rank sum test	ZnO-ns	ZnO/CuO-ns	ZnO/CuO-s
ZnO/CuO-ns	0.019	-	-
ZnO/CuO-s	0.013	0.013	-
ZnO-s	0.013	0.054	0.024

Figure 6 also shows the phase change for both nano-ZnO membrane and nano-ZnO/CuO membrane biosensors without capture antibody, but blocked with skimmed milk. The results were significantly lower than those obtained with the membranes containing antibody. Unsurprisingly the composition of the membranes was not statistically significant with respect to the biosensors with no capture antibody ($p=0.565$). This control did show a slight increase in signal output with increasing concentrations of CRP, which can be attributed to non-specific binding of CRP to proteins on the surface.

With antibody in the membranes, for both the nano-ZnO membrane and the nano-ZnO/CuO membrane, dose response relationships were evident from **Figure 6**. This indicates that the charge interactions of antigen binding with antibody resulted in

significantly larger output signals. It is speculated that there is increased charge accumulation due to the bound antigen on the surface compared with the non-specific binding of CRP.

The coefficient of variation (CV) was used to compare the variability of the data from ZnO with that from the ZnO/CuO membranes, with 200 ng anti-CRP. The average CV of the phase response at each concentration of CRP for the nano-ZnO/CuO (1:2) membrane is 9.6% compared with 15.6% for the nano-ZnO membrane, i.e. the ZnO/CuO membrane has better reproducibility. The ZnO/CuO membrane and ZnO membrane without sonication show CVs of 12.6% and 28.5% respectively. This demonstrates that the sonication stage of the fabrication process improved the reproducibility of nanoparticle membranes and the sonication process gave significantly higher results; for ZnO sonicated vs non-sonicated p=0.035 and for ZnO/CuO p=0.025.

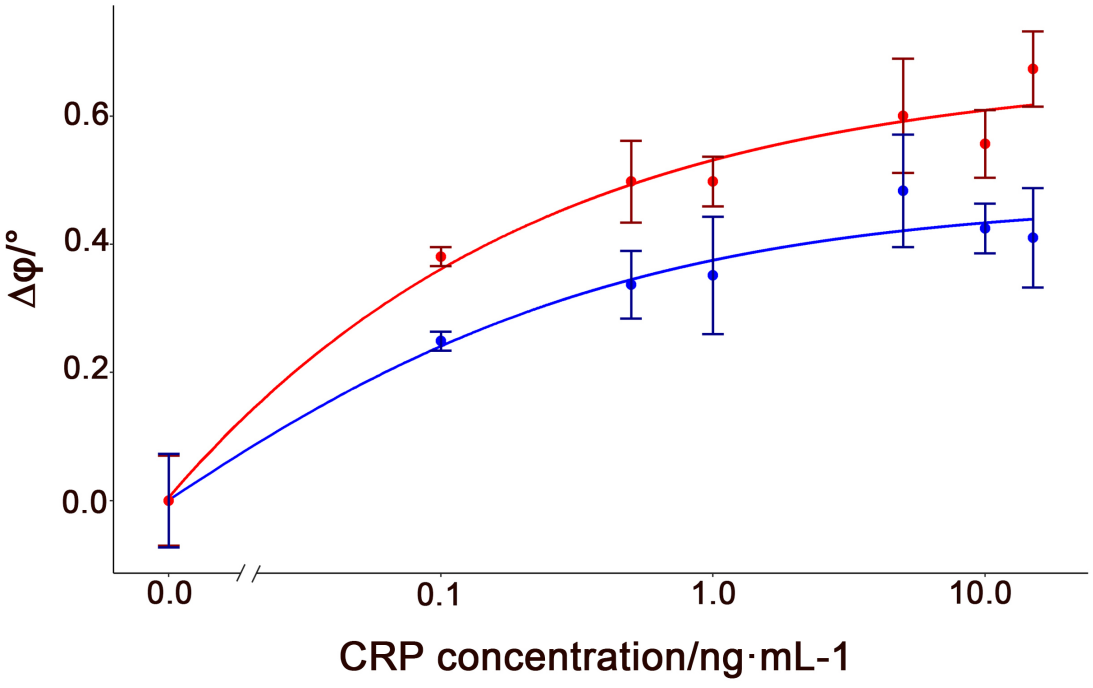

Fig. 7. Phase change/degree (Δφ/°) response versus antigen (CRP) concentration for sonicated nano-ZnO nitrocellulose membranes (red) and nano-ZnO/CuO nitrocellulose membranes (blue) with capture antibody (n=3) measured at the frequency of 100 Hz, - standard error bars are shown.

The 4-parameter logistic curve fits of the phase change data for both nano-ZnO and nano-ZnO/CuO membranes with sonication are shown in **Figure 7**. From these dose response curves, the regression line associated with the data from the nano-ZnO membranes has a R^2 value of 0.9645 and from the data of the nano-ZnO/CuO membranes, the R^2 value is 0.9744. It can be seen that the dose response curve with nano-ZnO membrane appears to become saturated at CRP concentrations above approximately 5 ng/mL, while with nano-ZnO/CuO membrane appears to saturate at approximately 15 ng/mL. The addition of CuO enabled an average enhancement of 1.4 times a greater signal across the range of 0.1 to 15 ng/mL. One explanation of this difference is the enhanced effect of nano-confinement in the ZnO/CuO membrane biosensor. This occurs when binding molecules are matched in size to the voids in the nanoparticle structure, resulting in charge screening due to the electric field distribution inside the structure [28]. **Figure 2** shows that the ZnO/CuO membranes have a closer packed structure with smaller voids, due to the smaller size of the CuO nanoparticles.

Table 2 shows the comparison of LoDs of nano-ZnO and nano-ZnO/CuO membranes with and without sonication. The LoD for the 1% nano-ZnO sonicated membranes with 200 ng anti-CRP was calculated to be 27 pg/ml, while the LoD for 1% nano-ZnO/CuO (1:2) sonicated membranes with 200 ng anti-CRP was 16 pg/ml. **Table 2** shows that the sonication has made a significant difference to the LoD on nano-ZnO/nitrocellulose membrane. The nano-ZnO/nitrocellulose membrane is a 92.6 times improvement, while nano-ZnO/CuO nitrocellulose membrane is a 1.25 times improvement. Both nano-ZnO/CuO nitrocellulose membranes with and without sonication show enhanced behaviours, i.e. lower limits of detection. It is hypothesised that the better detection limit and reduced enhancement due to sonication observed with the ZnO/CuO membranes is due to a decrease in the size to the voids in the nanoparticle structure compared with the ZnO membranes. This enhances the effect of nano-confinement, as described above, resulting in amplification of the signal and a smaller number of binding events being required to bring the signal above the noise threshold of the impedance instrument.

Table 2. Limits of detection of the phase change calibration curve for non-sonicated and sonicated ZnO and ZnO/CuO membranes.

LoD	Nano-ZnO non-sonicated membrane	Nano-ZnO sonicated membrane	Nano-ZnO/CuO non-sonicated membrane	Nano-ZnO/CuO sonicated membrane
Blank mean+3× standard deviation	2.5 ng/mL	27 pg/mL	20 pg/mL	16 pg/mL

In many articles in the literature, CRP is utilised as the model analyte to characterise new types of biosensor. A number of examples of sensitive CRP biosensors are listed in the supporting information, **Table S2**, and a selection is highlighted below. Dong et al. developed a paper-based microfluidic lateral flow immunoassay using gold nanoparticles to deliver a colorimetric output [7]. The key advancement presented related to the integration of the sensor with a smartphone using a microlens [7]. The assay was able to detect the target protein up to 2 μg/mL, however the detection limit was only 54 ng/mL and thus substantially inferior to the value presented in this work [7]. Justino et al. adopted the approach of enhancing sensitivity with nanoparticles, using carbon nanotubes on the sensor surface of a field-effect transistor. This showed improved performance for CRP detection, with a LoD of 0.1 ng/mL [34].

Impedimetric biosensors for detection of CRP have been developed by a number of research groups. For example, Bryan et al. presented a sensitive and reusable biosensor, using a well-established technique of analysing the charge transfer resistance to determine the CRP level [35]. A LoD of approximately 19 ng/mL was presented [35]. Yagati et al. also developed a faradaic impedimetric biosensor. This research team realised the benefit of using nanoparticles, utilising graphene oxide to achieve an improved LoD of 0.08 ng/mL [9]. However, compared with all these previous studies, the non-faradaic impedimetric nano-ZnO and nano-ZnO/CuO membrane biosensors presented in our paper, show excellent limits of detection.

The advantages of the non-faradaic impedimetric methodology are reinforced by reports in the literature. Lin et al. developed a non-faradaic biosensor for CRP

using a nano-porous alumina membrane as the sensor surface, rather than ZnO/CuO nanoparticles within a 3D membrane, as described in this paper. However, the approach also resulted in a low value for the LoD, i.e. 1 pg/mL. The advantages associated with the simplicity of measuring a change in capacitance were also highlighted [36]. Tanak et al. developed a non-faradaic electrochemical impedance spectroscopy-based biosensor for detection of CRP. In this case, 100 nm thin film of ZnO, deposited on the gold interdigitated electrodes was used and a LoD of 0.01 μg/mL in serum was achieved [37]. Neither of these studies utilised, ZnO or CuO nanoparticles nor a nanoporous membrane and they did not include an insulating layer between the electrodes and the sensor surface. However, the low LoD values, evidence the promising nature of the non-faradaic approach.

4. Conclusion

Both nano-ZnO nitrocellulose membrane and nano-ZnO/CuO nitrocellulose membrane biosensors can be fabricated using a simple and inexpensive colloidal sonication technique. Following fabrication, the cross section of nitrocellulose membrane contained increased densities of nanoparticles from the upper to the lower layers. The loading of ZnO and CuO nanoparticles within the membrane remained in proportion to the concentration of each type of nanoparticle within the original colloidal suspension. The sonication force is critical to assist the nanoparticles to be embedded into the lower layer of the membrane.

The addition of CuO nanoparticles of nano-ZnO/CuO nitrocellulose membrane biosensors showed enhancement of performance on impedance spectroscopy at 100 Hz across a concentration range of 0.1 ng/ml to 15 ng/mL CRP. The nano-ZnO nitrocellulose membrane biosensors revealed dose dependent responses with saturation occurring at approximately 5 ng/ml. The sonicated nano-ZnO and nano-ZnO/CuO nitrocellulose membranes showed limits of detection of 27 and 16 pg/mL respectively. Sonication during biosensor fabrication enhanced performance, with the nano-ZnO membrane showing an approximate 3-fold increase and the nano-ZnO/CuO nitrocellulose membrane showing an approximate 2-fold increase in phase change with sonication. The nano-ZnO/CuO nitrocellulose membrane with sonication showed the optimum results in terms of the highest

gradient and broadest detection range. Further work is being carried out to fully evaluate the biosensor and improve reproducibility, particularly through automating the fabrication process.

In addition to the simple and inexpensive fabrication methodology, which is compatible with large scale manufacture, and the excellent limits of detection, other advantages of this biosensor fabrication technique include the lack of contact between electrodes and measurement matrix and the fact that no redox active species are required. This biosensor fabrication methodology can be adapted to the measurement of any other analytes where an appropriate biological binding partner can be obtained and may be particularly suited to measurements, where high sensitivity or low sample volumes are required. These benefits make it a promising technique for adaption as a wearable biosensor.

Acknowledgment

PhD studentship was funded through the University of the West of England. The authors would like to thank Dr David Patton for help in producing the SEM images.

Conflict of Interest

None.

References

[1] N.R. Shanmugam, S. Muthukumar, S. Prasad, Ultrasensitive and low-volume point-of-care diagnostics on flexible strips - a study with cardiac troponin biomarkers, Sci. Rep. 6 (2016). https://doi.org/Artn 3342310.1038/Srep33423.

[2] Y.C. Shen, C.H. Yang, S.W. Chen, S.H. Wu, T.L. Yang, J.J. Huang, IGZO thin film transistor biosensors functionalized with ZnO nanorods and antibodies, Biosens Bioelectron. 54 (2014) 306–310. https://doi.org/DOI 10.1016/j.bios.2013.10.043.

[3] R.D. Munje, S. Muthukumar, A.P. Selvam, S. Prasad, Flexible nanoporous tunable electrical double layer biosensors for sweat diagnostics, Sci. Rep. 5 (2015). https://doi.org/Artn 1458610.1038/Srep14586.

[4] A.P. Selvam, K.M. Vattipalli, S. Prasad, Design of a High Sensitive Non-Faradaic Impedimetric Sensor, 2012 Annu. Int. Conf. Ieee Eng. Med. Biol. Soc. (2012) 3251–3254. https://doi.org/10.1109/EMBC.2012.6346658.

[5] J. Moon, G. Kim, S. Lee, A Gold Nanoparticle and Aflatoxin B1-BSA Conjugates Based Lateral Flow Assay Method for the Analysis of Aflatoxin B1, Materials (Basel). 5 (2012) 634–643. https://doi.org/10.3390/ma5040634.

[6] A. Malkoc, D. Probst, C. Lin, M. Khanwalker, C. Beck, C.B. Cook, J.T. La Belle, Enhancing Glycemic Control via Detection of Insulin Using Electrochemical Impedance Spectroscopy, J. Diabetes Sci. Technol. 11 (2017) 930–935. https://doi.org/10.1177/1932296817699639.

[7] M. Dong, J. Wu, Z. Ma, H. Peretz-Soroka, M. Zhang, P. Komenda, N. Tangri, Y. Liu, C. Rigatto, F. Lin, Rapid and Low-Cost CRP Measurement by Integrating a Paper-Based Microfluidic Immunoassay with Smartphone (CRP-Chip), Sensors (Basel). 17 (2017) 684. https://doi.org/10.3390/s17040684.

[8] A. Qureshi, J.H. Niazi, S. Kallempudi, Y. Gurbuz, Label-free capacitive biosensor for sensitive detection of multiple biomarkers using gold interdigitated capacitor arrays, Biosens. Bioelectron. 25 (2010) 2318–2323.

https://doi.org/10.1016/J.BIOS.2010.03.018.

[9] A.K. Yagati, J.C. Pyun, J. Min, S. Cho, Label-free and direct detection of C-reactive protein using reduced graphene oxide-nanoparticle hybrid impedimetric sensor, Bioelectrochemistry. 107 (2016) 37–44. https://doi.org/10.1016/j.bioelechem.2015.10.002.

[10] A. Ng, W.W. Tam, M.W. Zhang, C.S. Ho, S.F. Husain, R.S. McIntyre, R.C. Ho, IL-1β, IL-6, TNF- α and CRP in Elderly Patients with Depression or Alzheimer's disease: Systematic Review and Meta-Analysis, Sci. Rep. 8 (2018) 12050. https://doi.org/10.1038/s41598-018-30487-6.

[11] V. Panichi, M. Migliori, S. De Pietro, D. Taccola, B. Andreini, M.R. Metelli, L. Giovannini, R. Palla, The link of biocompatibility to cytokine production, Kidney Int. 58 (2000) S96–S103. https://doi.org/https://doi.org/10.1046/j.1523-1755.2000.07612.x.

[12] A. Janotti, C.G. Van de Walle, Fundamentals of zinc oxide as a semiconductor, Reports Prog. Phys. 72 (2009). https://doi.org/Artn 12650110.1088/0034-4885/72/12/126501.

[13] N.R. Shanmugam, S. Muthukumar, S. Prasad, A review on ZnO-based electrical biosensors for cardiac biomarker detection, Futur. Sci. OA. 3 (2017) FSO196-FSO196. https://doi.org/10.4155/fsoa-2017-0006.

[14] Z.L. Wang, Towards self-powered nanosystems: From nanogenerators to nanopiezotronics, Adv. Funct. Mater. 18 (2008) 3553–3567. https://doi.org/10.1002/adfm.200800541.

[15] M. Ahmad, M.A. Iqbal, J. Kiely, R. Luxton, M. Jabeen, Enhanced output voltage generation via ZnO nanowires (50 nm): Effect of diameter thinning on voltage enhancement, J. Phys. Chem. Solids. 104 (2017) 281–285. https://doi.org/10.1016/J.JPCS.2017.01.006.

[16] B.K. Meyer, A. Polity, D. Reppin, M. Becker, P. Hering, P.J. Klar, T. Sander, C. Reindl, J. Benz, M. Eickhoff, C. Heiliger, M. Heinemann, J. Bläsing, A. Krost, S. Shokovets, C. Müller, C. Ronning, Binary copper oxide

semiconductors: From materials towards devices, Phys. Status Solidi. 249 (2012) 1487–1509. https://doi.org/10.1002/pssb.201248128.

[17] N.M. Vuong, N.D. Chinh, B.T. Huy, Y.-I. Lee, CuO-Decorated ZnO Hierarchical Nanostructures as Efficient and Established Sensing Materials for H2S Gas Sensors, Sci. Rep. 6 (2016) 26736. http://dx.doi.org/10.1038/srep26736.

[18] P.-J. Lu, W.-E. Fu, S.-C. Huang, C.-Y. Lin, M.-L. Ho, Y.-P. Chen, H.-F. Cheng, Methodology for sample preparation and size measurement of commercial ZnO nanoparticles, J. Food Drug Anal. 26 (2018) 628–636. https://doi.org/10.1016/J.JFDA.2017.07.004.

[19] Y.C. Zhang, T. Yang, N. Zhou, W. Zhang, K. Jiao, Nano Au/TiO(2) hollow microsphere membranes for the improved sensitivity of detecting specific DNA sequences related to transgenes in transgenic plants, Sci. China Ser. B-Chemistry. 51 (2008) 1066–1073. https://doi.org/10.1007/s11426-008-0116-2.

[20] M.H. Al-Hinai, P. Sathe, M.Z. Al-Abri, S. Dobretsov, A.T. Al-Hinai, J. Dutta, Antimicrobial Activity Enhancement of Poly(ether sulfone)Membranes by in Situ Growth of ZnO Nanorods, ACS Omega. 2 (2017) 3157–3167. https://doi.org/10.1021/acsomega.7b00314.

[21] K.S. Lee, C.H. Kim, S.W. Jeong, Y. Song, N.H. Bae, S.J. Lee, K.G. Lee, Ultrasonic fabrication of flexible antibacterial ZnO nanopillar array film, Colloids Surfaces B Biointerfaces. 170 (2018) 172–178. https://doi.org/10.1016/J.COLSURFB.2018.06.007.

[22] N. Widiarti, J.K. Sae, S. Wahyuni, Synthesis CuO-ZnO nanocomposite and its application as an antibacterial agent, IOP Conf. Ser. Mater. Sci. Eng. 172 (2017) 012036. http://stacks.iop.org/1757-899X/172/i=1/a=012036.

[23] V. Tiwari, N. Mishra, K. Gadani, P.S. Solanki, N.A. Shah, M. Tiwari, Mechanism of Anti-bacterial Activity of Zinc Oxide Nanoparticle Against Carbapenem-Resistant Acinetobacter baumannii, Front. Microbiol. 9 (2018) 1218. https://doi.org/10.3389/fmicb.2018.01218.

[24] R. Ahmad, N. Tripathy, M.-S. Ahn, K.S. Bhat, T. Mahmoudi, Y. Wang, J.-Y. Yoo, D.-W. Kwon, H.-Y. Yang, Y.-B. Hahn, Highly Efficient Non-Enzymatic Glucose Sensor Based on CuO Modified Vertically-Grown ZnO Nanorods on Electrode, Sci. Rep. 7 (2017) 5715. https://doi.org/10.1038/s41598-017-06064-8.

[25] N. Tripathy, D.-H. Kim, Metal oxide modified ZnO nanomaterials for biosensor applications, Nano Converg. 5 (2018) 27. https://doi.org/10.1186/s40580-018-0159-9.

[26] L. Cao, J. Kiely, M. Piano, R. Luxton, A Copper Oxide/Zinc Oxide Composite Nano-Surface for Use in a Biosensor, Materials (Basel). 12 (2019). https://doi.org/10.3390/ma12071126.

[27] L. Cao, J. Kiely, M. Piano, R. Luxton, Facile and inexpensive fabrication of zinc oxide based bio-surfaces for C-reactive protein detection, Sci. Rep. 8 (2018) 12687. https://doi.org/10.1038/s41598-018-30793-z.

[28] R.D. Munje, S. Muthukumar, S. Prasad, Lancet-free and label-free diagnostics of glucose in sweat using Zinc Oxide based flexible bioelectronics, Sensors and Actuators B-Chemical. 238 (2017) 482–490. https://doi.org/10.1016/j.snb.2016.07.088.

[29] A. Panneer Selvam, S. Muthukumar, V. Kamakoti, S. Prasad, A wearable biochemical sensor for monitoring alcohol consumption lifestyle through Ethyl glucuronide (EtG) detection in human sweat, Sci. Rep. 6 (2016) 23111. https://doi.org/10.1038/srep23111.

[30] V. Edwards, Electron Theory, EDTECH, 2018. https://books.google.co.uk/books?id=GeTEDwAAQBAJ.

[31] C. Wang, C. Wang, B. Feng, Research progress on site-oriented and three-dimensional immobilization of protein, Mol. Biol. (New York). 49 (2015) 1–20. https://doi.org/10.1134/S0026893315010173.

[32] E. Juntunen, Lateral flow immunoassays with fluorescent reporter technologies, University of Turku, PhD thesis, 2018.

[33] D. Kinnamon, R. Ghanta, K.-C. Lin, S. Muthukumar, S. Prasad, Portable biosensor for monitoring cortisol in low-volume perspired human sweat, Sci. Rep. 7 (2017) 13312. https://doi.org/10.1038/s41598-017-13684-7.

[34] C.I.L. Justino, A.C. Freitas, J.P. Amaral, T.A.P. Rocha-Santos, S. Cardoso, A.C. Duarte, Disposable immunosensors for C-reactive protein based on carbon nanotubes field effect transistors, Talanta. 108 (2013) 165–170. https://doi.org/10.1016/J.TALANTA.2013.03.007.

[35] T. Bryan, X. Luo, P.R. Bueno, J.J. Davis, An optimised electrochemical biosensor for the label-free detection of C-reactive protein in blood, Biosens. Bioelectron. 39 (2013) 94–98. https://doi.org/10.1016/j.bios.2012.06.051.

[36] K.-C. Lin, V. Kunduru, M. Bothara, K. Rege, S. Prasad, B.L. Ramakrishna, Biogenic nanoporous silica-based sensor for enhanced electrochemical detection of cardiovascular biomarkers proteins, Biosens. Bioelectron. 25 (2010) 2336–2342. https://doi.org/10.1016/J.BIOS.2010.03.032.

[37] A.S. Tanak, B. Jagannath, Y. Tamrakar, S. Muthukumar, S. Prasad, Non-faradaic electrochemical impedimetric profiling of procalcitonin and C-reactive protein as a dual marker biosensor for early sepsis detection, Anal. Chim. Acta X. 3 (2019) 100029. https://doi.org/https://doi.org/10.1016/j.acax.2019.100029.